

Article

High-Efficiency Catalysis of Peroxymonosulfate by MgO for the Degradation of Organic Pollutants

Qian Peng^{1,2}, Xuekun Tang^{1,2}, Kun Liu^{1,2,*}, Xianping Luo³, Dongsheng He⁴, Ying Dai^{1,2} and Ganghong Huang^{1,2}

¹ School of Minerals Processing and Bioengineering, Central South University, Changsha 410083, China; pengqianhn@163.com (Q.P.); txk0797@126.com (X.T.); yingdaiyeah@163.com (Y.D.); ghhuang@csu.edu.cn (G.H.)

² Hunan Key Laboratory of Mineral Materials and Application, Central South University, Changsha 410083, China

³ School of Resource and Environmental Engineering, Jiangxi University of Science and Technology, Ganzhou 341000, China; lxp9491@163.com

⁴ Xingfa School of Mining Engineering, Wuhan Institute of Technology, Wuhan 430074, China; hds@wit.edu.cn

* Correspondence: kliu@csu.edu.cn

Received: 15 November 2019; Accepted: 16 December 2019; Published: 18 December 2019



Abstract: In the study, magnesium oxide (MgO) was used to catalyze peroxymonosulfate (PMS) for the degradation of organic pollutants for the first time. According to the single-factor experiment results, it was determined that MgO could efficiently catalyze PMS to degrade organic matters in a wide range of pH values. Based on radical quenching experiments and electron spinning resonance spectra, singlet oxygen was identified to be the crucial reactive species. Importantly, the oxygen vacancy on the surface of MgO was determined as the key active site, which accelerated the decomposition of PMS to produce singlet oxygen. This study provides an interesting insight into the novel and ignored catalyst of MgO for the highly efficient activation of PMS, which will greatly benefit the Fenton-like catalytic degradation of organic wastewater.

Keywords: Fenton-like catalysis; peroxymonosulfate; MgO; oxygen vacancy; singlet oxygen

1. Introduction

Effluents from textile industries have caused extensive public concern, since a variety of organic compounds and toxic substances are difficult to decolorize due to their complex structure and synthetic origin, which flow into the river and threaten people's health [1–3]. Therefore, the effective treatment of dye wastewater is of highly concern [4]. Through extensive research on the removal of various organic pollutants, many treatment methods have been developed, such as physical methods (adsorption, coagulation, and membrane separation), chemical methods (ozone oxidation, electrochemical and wet oxidation, and advanced catalytic oxidation), and biological methods (aerobic biological treatment, anaerobic biological treatment, and anaerobic–aerobic combined biological treatment) [5–7]. Among these methods, advanced oxidation process (AOP) is considered to be the most promising method because of its high removal efficiency and wide range of applications [8].

Advanced oxidation processes (AOP) basing on highly reactive oxygen species, including hydroxyl radicals, superoxide anion radicals, sulfates radical, and singlet oxygen, has shown great potential for the removal of emerging pollutants [9,10]. The radicals initially used and their precursors in decontamination techniques are hydroxyl radicals and Fenton's reagents (hydrogen peroxide and iron ions) [11]. However, the practical application is limited because of poor selectivity, secondary pollution, narrow pH range, reagent storage, and sludge removal [12,13]. In 2003, peroxymonosulfate (PMS), instead of hydrogen peroxide, was used as a strong oxidant, and Co^{2+} was used a catalyst

to achieve efficient degradation of organic pollutants, which marked a new phase in the study of Fenton-like reactions that compensate for the disadvantages of hydrogen peroxide [14]. Therefore, in the following decades, the persulfate-based Fenton-like catalytic oxidation process has received widespread attention from researchers all over the world [15]. Peroxymonosulfate can be efficiently activated via thermal radiation, UV light, ultraviolet, base and transition metals cation (Co^{2+} , Ce^{3+} , Ag^+ , Fe^{2+} , Fe^{3+} , Ni^{2+} , Ru^{3+} , Mn^{2+} , etc.), or oxides [16]. However, the high energy requirements of heat and ultraviolet light exposure, the risk of metal toxicity and secondary pollution limit the further industrial application of these activation methods [17]. Therefore, the catalysis of PMS to degrade organic contaminants by new catalysts has attracted more and more attention recently. Fan's group presented a simple one-pot synthetic approach for the Mn-doped graphite-phase carbon nitride ($\text{g-C}_3\text{N}_4$), which catalyzed peroxymonosulfate to generate superoxide radicals and singlet oxygen for acetaminophen degradation [18]. Liu's group catalyzed PMS by supporting Fe_3O_4 nanoparticles and nanoflower-like MnO_2 layer by layer on the surface of porous diatomite or silica nanofiber. The high specific area of the core-shell nanocomposites made it easier for PMS and organic pollutants to contact with the catalysts, and the synergistic effect between MnO_2 and Fe_3O_4 increased the activation performance of the catalysts [8,19,20]. Huang's group reported iron-copper bimetal doped mesoporous $\text{g-Al}_2\text{O}_3$ catalyzed PMS to effectively degrade 4-chlorophenol, finding that the Al-O-Fe and Al-O-Cu bonds formed by Fe and Cu doping into the framework of $\text{g-Al}_2\text{O}_3$ were the key structures for high activity of the catalyst [21]. Although these catalysts can activate PMS to some extent as well, complex synthesis and lack of universality are also the obstacles for them to realize industrial application [22]. Thus, it is very important and urgent to develop a low-cost, high-efficiency, and easy-to-implement catalyst to activate persulfate for the degradation of organic pollutants.

To the best of our knowledge, no study has been reported on the application of magnesium oxide (MgO) to catalyze PMS. Moreover, it is well-known that MgO, as a very common and simple chemical, is available in large quantities, cheap, and environmentally friendly, and it can rapidly realize large-scale water-purification applications. In our present work, the effect of MgO on the degradation of organic pollutants by catalyzing PMS is reported for the first time, and the influencing factors of the catalytic process, including time, temperature, concentration of pollutants, dosage of MgO and PMS, dissolved oxygen, and pH value, are systematically investigated. The possible catalytic mechanism of MgO is illustrated based on the effect of oxygen vacancy and hydroxyl on catalytic degradation, the stability and recyclability of MgO are also studied. Our results confirm the high efficiency of MgO catalysis and describe the catalytic process reasonably, which will be of great practical significance.

2. Materials and Methods

2.1. Reagents and Materials

All chemical reagents and organic solvents were analytical grade and were used without further purification. Peroxymonosulfate (PMS, $\text{KHSO}_5 \cdot 0.5\text{KHSO}_4 \cdot 0.5\text{K}_2\text{SO}_4$), MgO (FCC crystal structure, average diameter of about 50 nm), Methyl Orange, Malachite Green, Acid Red 73, and superoxide dismutase were purchased from Aladdin Bio-Chem Technology Co., Ltd. (Shanghai, China). Methylene Blue (MB), NaOH, methanol, tert-butanol, and furfuryl alcohol were obtained from Sinopharm Chemical Reagent Co., Ltd. (Shanghai, China). Deionized water was used throughout the whole study. As a contrast, two kinds of high-pure MgO, with average particle size about 1 and 10 μm , were also used in experiments (Figure S1).

2.2. Characterization

The X-ray powder diffraction (XRD) (BRUKER AXS GMBH, Karlsruhe, Germany) patterns of the samples were measured by Bruker AXS D8 Advance diffractometer with copper $\text{K}\alpha$ source ($\lambda = 0.15418 \text{ nm}$). The X-ray photoelectron spectroscopy (XPS) measurements were carried out on a Thermo Fisher Escalab 250 Xi electron spectrometer (Thermo Fisher Scientific, Waltham, MA, USA).

Electron spin resonance (ESR) experiments were carried out by using a Bruker A300 ESR spectrometer (Bruker (Beijing) Technology Co., Ltd., Beijing, China) with DMPO or TEMP as a spin-trapping agent. The steady-state photoluminescence (PL) spectra of the samples were conducted on a Hitachi F-4600 fluorescence spectrophotometer (Hitachi hi-tech co., Ltd., Shanghai, China), with excitation at 325 nm [23].

2.3. Evaluation of Catalytic Performance

All experiments were carried out in a constant-temperature water bath, in a 250 mL flask. Usually, MgO was uniformly dispersed in a 100 mL of Methylene Blue (MB) solution (100 mg/L), with constant stirring. The solution was quickly adjusted to specific initial pH, with NaOH powder, and concentrated H₂SO₄ solution. Then PMS was added into the solution, to activate the catalytic reaction. After a certain period of reaction, the water sample was collected, using a syringe with a filter (0.22 μm), and analyzed with a UV-2600 spectrophotometer, at an absorption wavelength of 664 nm [24]. Under the same experimental procedure, the effects of MB concentration, temperature, pH value, and dosage of PMS and MgO on the catalytic reaction were investigated.

The filtered catalyst after MB degradation was collected and used for the next catalytic reaction cycle. The experimental procedure and parameters were the same as those mentioned above.

3. Results and Discussion

3.1. Catalytic Degradation Effect by PMS/MgO System

3.1.1. Catalytic Activity of MgO

The efficiency of MgO catalysis for PMS was determined by using Methylene Blue (MB) as a target pollutant. As shown in Figure 1, bare MgO has only a weak adsorptive effect on MB, and naked PMS leads to only about 40% degradation of MB in 60 min. Surprisingly, simultaneous addition of MgO and PMS brings about a nearly complete degradation of MB, with a degradation of 99.4% in 20 min. It can be concluded that MgO can effectively catalyze PMS to accelerate the decomposition of MB. By contrast, the catalysis efficiency for PMS by various Mg-containing catalysts also were studied, including Mg(OH)₂, Mg, and MgCl₂, under the same experimental conditions. Catalytic degradation experiments were carried out by using the same magnesium quality of MgO, Mg(OH)₂, Mg, and MgCl₂. The degradation processes of MB by PMS/Mg and PMS/Mg²⁺ systems are like that of bare PMS, indicating that Mg and Mg²⁺ can hardly catalyze PMS. However, interestingly, the PMS/Mg(OH)₂ system demonstrates non-negligible activity, although it is not as good as the PMS/MgO system, which may be due to the catalytic effect of hydroxyl in Mg(OH)₂. As reported in the previous literature, the hydroxyl is an effective catalyst toward PMS in the pH range of 6.2 to 10.86, especially at pH > 9 [9].

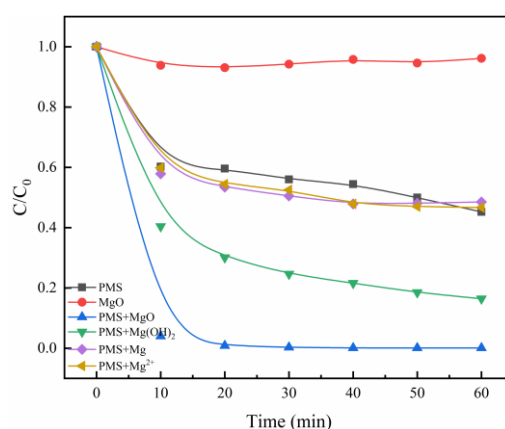


Figure 1. The degradation of MB by different Mg catalysts. Control conditions: (MB) = 10 mg/L, (PMS) = 0.8 g/L, (MgO) = 0.4 g/L, (Mg(OH)₂) = 0.58 g/L, (Mg) = 0.24 g/L, (MgCl₂) = 0.95 g/L, T = 25 °C.

3.1.2. Influence of Process Variables

To further investigate the catalytic activity of the MgO, the degradation efficiencies of MB by PMS/MgO under different process variables were investigated. Figure 2a shows the comparison of MB at different initial concentrations. In the initial concentration range of 10–100 mg/L, MB is completely degraded within 60 min, indicating that MgO has a very high catalytic efficiency for PMS to degrade MB with various concentration levels. Generally, MB in high concentration is difficult to be catalytically degraded [25]. As a result, in many previous studies about catalytic degradation, the MB concentration is normally not more than 20 mg/L. This is a very gratifying result that greatly enhances the feasibility of practical application in actual wastewater. However, with the increase of MB concentration from 10 to 100 mg/L, the degradation rate decreases gradually. On the one hand, more dye molecules correspondingly need more time to degrade. On the other hand, more dye molecules adsorb on the surface of MgO at higher concentrations, which hinders the contact between PMS and MgO to inhibit the generation of active oxygen species.

Figure 2b shows the degradation efficiency of MB depends heavily on the dosage of PMS. The top control curve shows that MB can hardly be degraded without the addition of PMS. When the dosage of PMS is less than 0.8 g/L, it can be seen that the degradation efficiency of MB increases sharply with the increase of the dosage. Then, with the increase of PMS dosage to 2 g/L, the degradation efficiency increases slowly. Figure 2c presents the effect of MgO dosage on MB degradation, which is very similar to the Figure 2b. A key MgO quantity of 0.4 g/L is determined. The degradation efficiency of MB exceeds 90% when the dosage of MgO is 0.4 g/L. However, over this dosage, the degradation efficiency of MB increases very slowly. The control curve shows that the PMS can decompose itself to generate active species to degrade MB inefficiently, without the catalysis of MgO [26]. Figure 2b,c confirms that MgO is an extremely efficient catalyst for PMS, and points out that the dosages of MgO and PMS are crucial parameters for MB degradation and reasonable dosages can ensure the best effect.

The effect of reaction temperature on the degradation of MB was investigated, and the results are shown in Figure 2d. As we all known, the rate of reaction depends on the probability of effective collision between molecules. The increase in temperature will greatly increase the collision between molecules, so the effective collision will increase, and the reaction rate will be faster [27]. As it can be seen from Figure 2d, temperature has a large effect on the decolorization efficiency of MB, and an increase in temperature (30, 35, and 40 °C) accelerates discoloration. Temperature, which increases the reaction rate between PMS and MgO and the generation rate of active oxygen species, exerts a strong effect on the degradation of MB.

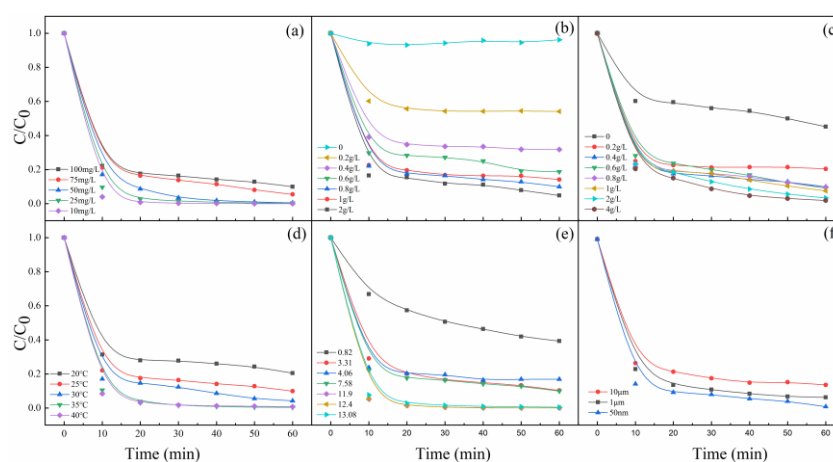


Figure 2. Effects of (a) MB concentration, (b) PMS dosage, (c) MgO dosage, (d) reaction temperature, (e) pH values, and (f) particle sizes of MgO on MB degradation. Control conditions: (MB) = 100 mg/L, (PMS) = 0.8 g/L, (MgO) = 0.4 g/L, pH = 7, T = 25 °C.

Figure 2e presents the effect of initial pH of the solution (from about 1 to about 13) on MB degradation. It is noticed that the degradation rate of MB changes little when the pH values are between 3.31 and 7.58, while it decreases dramatically when the pH is 0.82 and increases greatly when the pH is varied from 11.9 to 13.08. These experimental phenomena mean that the degradation of MB is significantly affected by the solution pH value. For one thing, the hydroxyl in the solution can effectively catalyze PMS, especially at $\text{pH} \geq 9$, as presented in the previous literature [9]. For another thing, at low pH value, H^+ can scavenge the generation of active oxygen species and accelerate the dissolution of magnesium oxide, resulting in a decrease in the degradation rate of MB [28]. A stable and efficient degradation efficiency of MB is obtained in a wide pH range (from 3.31 to 13.08) in the experiment, which maybe because the active sites on the surface of MgO are independent of the concentration of H^+ or OH^- . At the same time, we also studied the effect of the particle size of MgO on the degradation efficiency of MB by introducing micron-sized MgO with average particles about 1 and 10 μm . As shown in Figure 2f, it is found that the smaller the particle size, the higher the degradation efficiency, which is due to the fact that, the smaller the particle size is, the higher the specific surface area and the higher the concentration of the active sites [29].

To test the recyclability of MgO, the catalyst was collected by filtration after the complete degradation of MB, and then the reaction was reinitiated by adding fresh PMS and dye solution. As it can be seen from Figure 3, the catalyst remains close to 100% high recyclability after five cycles. Meanwhile, the MgO after five cycles was detected by XRD, which was in good agreement with that of fresh MgO (Figure S2), indicating that MgO is a stable and effective catalyst. In addition to MB, the degradation effects of the PMS/MgO system on different dyes, including Methyl Orange (MO), Malachite Green (MG), and Acid Red 73 (AR73), were also tested. As shown in Figure S3, the MO and MG can be completely degraded in 20 min, and the AR73 also can be degraded about 90% in 60 min, demonstrating the high efficiency and universality of the PMS/MgO catalytic degradation system.

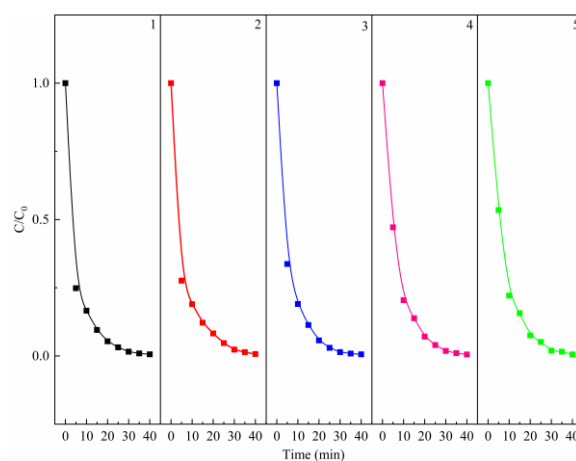


Figure 3. Recyclability of the MgO catalyst for the degradation of MB. Control conditions: (PMS) = 0.8 g/L, (MgO) = 0.4 g/L, (MB) = 50 mg/L, T = 25 °C.

3.2. Catalytic Degradation Process and Mechanisms of PMS/MgO System

3.2.1. Determination of Active Oxygen Species

The good degradation effect of MB is ascribed to the catalysis of PMS by MgO, to generate the reactive oxygen species. In order to determine the contribution of different reactive oxygen species, different radical scavengers were added to the PMS/MgO system, including methanol for sulfate radical ($\text{SO}_4^{\cdot-}$) [30], tert-butanol (TBA) for hydroxyl radical ($\cdot\text{OH}$) [31], superoxide dismutase for superoxide anion radical ($\text{O}_2^{\cdot-}$) [32], and furfuryl alcohol for singlet oxygen ($^1\text{O}_2$) [33]. As shown in Figure 4, the addition of tert-butanol (TBA) did not inhibit MB degradation, even though a large amount of tert-butanol (TBA) (TBA/PMS = 300, shown in Figure S4a) was added, suggesting that the hydroxyl

radical may not be reactive oxygen species. A similar result is obtained when methanol, a scavenger of both hydroxyl radical and sulfate radical, is added to the PMS/MgO system, shown in Figure 4 and Figure S4b. This indicates that neither hydroxyl radical nor sulfate radical is the reactive oxygen species involved in the PMS/MgO system, which is different from the ordinary PMS catalytic process. Generally, sulfate and hydroxyl radicals are considered to be reactive oxygen species produced during the catalysis of PMS.

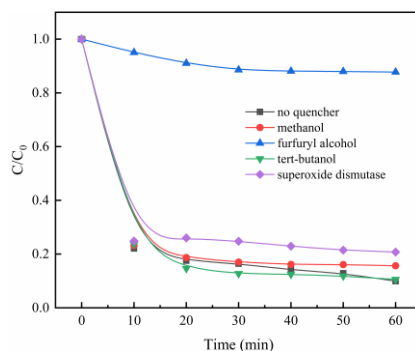


Figure 4. Effects of the radical scavengers on MB degradation (a) methanol, (b) tert-butanol (TBA), (c) SOD, and (d) furfuryl alcohol. Control conditions: (MB) = 100 mg/L, (PMS) = 0.08 g, (MgO) = 0.04 g, pH = 7, T = 25 °C.

Recently, it was reported that the persulfate system can produce superoxide anion radicals ($O_2^{\cdot-}$) and singlet oxygen (1O_2), which are less interfered by the background component of water and more selective than $SO_4^{\cdot-}$ and $\cdot OH$, thereby increasing the persulfate utilization rate [34]. The degradation of MB is slightly suppressed when superoxide dismutase is added to the reaction mixture. However, as seen in the Figure 4 and Figure S4d, when furfuryl alcohol is added to the solution, the degradation of MB is almost entirely restrained. This directly indicates that singlet oxygen and superoxide radicals are involved in MB degradation, and the singlet oxygen plays a key role.

In order to further confirm the active oxygen species involved in the PMS/MgO system, electron spin resonance (ESR) was performed to determine which kinds of free radicals existed during the oxidation reaction. Since a radical has a very short half-life, its direct detection is impossible. However, a radical can be trapped through its reaction with a spin-trap agent 5,5-dimethyl-1-pyrroline-N-oxide (DMPO) or 2,2,6,6-tetramethylpiperidine (TEMP), to form a DMPO-X or TEMP-X radical, which has much longer half-life [35,36]. DMPO can react with a hydroxyl radical, sulfate radical, and superoxide anion radical to form DMPO-OH, DMPO-SO₄, and DMPO-OOH spin-adducts, respectively [37]. TEMP can capture singlet oxygen, to form spin-adduct TEMPO [38,39]. These paramagnetic products can be detected by ESR, and clear and readable ESR spectra can be obtained in order to identify the existence of free radicals. First, the DMPO was used in the PMS/MgO-aqueous system, to trap radicals, as shown in Figure 5a. Only the characteristic signal of DMPO-OH adduct with strength of 1:2:2:1 is observed, pointing out that only hydroxyl radical is generated. The signal of sulfate radicals cannot be found, most likely owing to its absence or low concentration [40]. In order to avoid the reaction of DMPO with hydroxyl radical, the DMPO was added to the PMS/MgO-ethanol system, to detect superoxide radicals, as presented in Figure 5b. Six characteristic peaks of superoxide radicals are observed, revealing the presence of superoxide radicals in the reaction systems. Subsequently the TEMP was added into the PMS/MgO-aqueous system, as seen in Figure 5c; the ESR spectrum shows a 1:1:1 triplet signal characteristic of TEMPO adducts, indicating the presence of singlet oxygen in the reaction system.

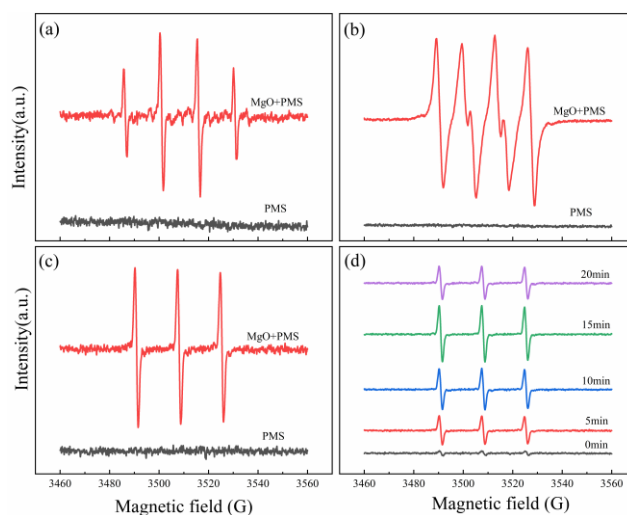


Figure 5. ESR spectra of trapped radical adducts in different systems. (a) DMPO in PMS/MgO-aqueous system, (b) DMPO in PMS/MgO-ethanol system, (c) TEMP in PMS/MgO-aqueous system, and (d) singlet oxygen adduct captured at different times in PMS/MgO system.

From the quenching experiment, it can definitely be determined that the singlet oxygen is the crucial reactive oxygen species. In order to better understand the production process of singlet oxygen, we detected the singlet oxygen in the period of 0–20 min by ESR, as shown in Figure 5d. As soon as the detection system starts to react, the 1:1:1 triplet signal characteristic of TEMPO spin-adduct is detected. Moreover, before 15 min, the signal intensity gradually increases with the progress of the reaction, further indicating that singlet oxygen is the crucial active oxygen species and is produced continuously in the reaction process. The signal intensity increases significantly at the initial stage of the reaction, which may be due to the rapid catalytic decomposition of PMS by MgO. After 15 min, the signal intensity begins to decrease, obviously, which means that a lot of PMS is reacted, thus reducing the concentration of free radicals. The degradation efficiency of organic compounds is mainly dependent on the concentration of free radicals. Therefore, the degradation rate of organic molecules is fast in the early stage and slow in the late stage, which is in good agreement with the previous experimental results shown in Figure 2. As a result, these spin trap experiments further confirm that in the PMS/MgO system, hydroxyl radicals, superoxide radicals and singlet oxygen are generated, and the singlet oxygen is the crucial reactive oxygen species.

In theory, there are usually two ways to produce singlet oxygen. On the one hand, dissolved oxygen molecules, as the precursor, is transformed into singlet oxygen due to the energy transfer in the catalytic process [41]. On the other hand, the singlet oxygen can be formed through the cleavage and disproportionation of peroxide bond (O–O) in PMS [34]. In order to determine the origin of the singlet oxygen in the system, argon was continuously introduced into the reaction system to reduce the content of dissolved oxygen from normal level of about 7 mg/L to less than 0.1 mg/L. Under this condition, the effect of the degradation of MB by PMS/MgO was examined to determine the influence of dissolved oxygen on the generation of singlet oxygen. The results in Figure S5 show that two degradation curves are almost the same, although the content of dissolved oxygen is quite different, which indicates that the singlet oxygen has nothing to do with the dissolved oxygen and its production does not derive from oxygen molecules. As a result, it can be reasonably concluded that the singlet oxygen originates from the PMS itself.

3.2.2. Effect of Hydroxyl in Solution on Catalytic Process

Previous reports have shown that PMS can be catalyzed by alkali, and the catalytic process of PMS is related to the hydroxyl content in solution [9]. Therefore, in order to determine the effect of hydroxyl in the solution on PMS/MgO catalysis process, a set of designed experiments were performed

under different initial pH values. It can be seen from the degradation curves under various pH values (Figure 2e) that the plot from 20 to 60 min is flat. Therefore, the average value of 20, 40, and 60 min is used to represent the degradation efficiency. The initial pH value of MB solution was first adjusted to a set value by sulfuric acid and sodium hydroxide, and then the PMS was added into solution, with or without MgO.

The effect of hydroxyl in solution on catalysis process can be judged by comparing the degradation differences between PMS/MgO and bare PMS systems. The results are shown in Figure 6. When the initial pH value is about 1, the degradation efficiency in both systems is similar and not good, but the PMS/MgO system is slightly better. On the one hand, this is due to the decomposition of PMS is inhibited at low pH value [29]. On the other hand, MgO is alkaline oxide that is unstable under acidic conditions. As shown in Figure S6, the dissolution rate of MgO gradually increases with the decrease of pH value, and MgO almost completely dissolves when the pH is about 1. Then, with the increase of pH value to about 3, the degradation efficiency of PMS/MgO system increases dramatically, and the proportion of residual MB decreases rapidly from about 40% to about 10%. As a reference, the degradation efficiency of bare PMS system is slowly improved. As reported, the catalytic effect of hydroxyl group to PMS can only be achieved under alkaline conditions [9]. However, the excellent degradation effect of PMS/MgO system in the range of pH of 3 to 11 indicates that MgO contributes an extra excellent catalytic effect in addition to hydroxyl groups. Subsequently, the catalytic efficiency of both systems remains stable in the pH range of 3 to 11, namely, MB residual rates are kept at about 10% and 40% in PMS/MgO and bare PMS systems, respectively. Finally, when the pH value is more than 12, the degradation efficiency of bare PMS system increases greatly, while that of PMS/MgO system increases gradually. Ultimately, the degradation efficiencies of both systems are completely equal. At this point, the hydroxyl group dominates the catalysis.

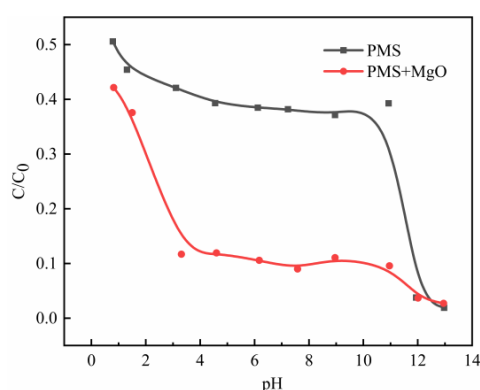


Figure 6. Effect of initial pH values on degradation in PMS/MgO and bare PMS systems. Control conditions: (MB) = 100 mg/L, (PMS) = 0.08 g, (MgO) = 0.04 g, T = 25 °C.

This phenomenon indicates that the hydroxyl in solution is quite effective catalyst toward PMS, as reported in previous literatures. Meanwhile, the MgO can significantly and steadily improve the degradation effect, which directly confirms the important catalytic role of MgO in addition to hydroxyl in a very wide range of pH values. In general, both hydroxyls in solution and MgO can catalyze PMS in PMS/MgO system. The catalysis mechanism has been explained clearly for hydroxyl in solution, but it is unknown for MgO. Next, we try to explain the catalytic mechanism of MgO for PMS.

3.2.3. Effect of Hydroxyl and Oxygen Vacancy in the MgO Surface on Catalytic Process

Hydroxyl in solution can catalyze PMS, and, recently, it has been found that hydroxyl group in minerals can also catalyze PMS [22]. Therefore, the hydroxyl group on MgO surface should also have a certain catalytic effect. According to previous reports, there is a large amount of hydroxyl groups on the surface of MgO due to the adsorbed H₂O molecules from air [42]. In order to investigate the catalysis of hydroxyl group on the surface, the MgO was calcined at 600 °C for 2 h in argon atmosphere,

to completely remove the hydroxyl groups. Then the calcined MgO was preserved in argon and used to catalyze PMS for the degradation of MB. At the same time, a comparative experiment was carried out with normal MgO. Considering the regeneration of hydroxyl groups on the surface of MgO in water, only the degradation in first ten minutes was used to illustrate the effect of surface hydroxyl groups, as shown in Figure S7. Both degradation curves show almost-parallel trends, but the degradation efficiency of calcined MgO is slightly worse. This indicates that the surface hydroxyl group of MgO has a slight catalytic effect on PMS. In order to further confirm that the catalytic effect of surface hydroxyl group is very weak, three kinds of MgO with different particle sizes (50 nm, 1 μm , and 10 μm) were calcined and then catalyzed PMS according to abovementioned procedure. As shown in Figure S8, these calcined MgO can still catalyze PMS to degrade MB, and the smaller the particle size, the better the catalytic performance, which is consistent with that of MgO particles without calcination, which are presented in Figure 2f. It can be determined that, in addition to the hydroxyl group, there is another factor in the MgO surface that plays a key role in the catalysis of PMS, and this factor is closely related to particle size.

We turn our eyes to the surface defects on MgO. Many results show that the smaller the size of the catalyst particles, the larger the specific surface area, the more surface defects and the higher the catalytic activity [43]. The X-ray photoelectron spectroscopy (XPS) provides information about elemental composition and valence state of sample surface [19,44], so the XPS was used to study above three kinds of MgO with different particle sizes.

Figure 7 shows the XPS spectra of MgO at 50 nm (a and b), MgO at 1 μm (c and d), and MgO at 10 μm (e and f). In the full scan of samples (a, c, and e), only the characteristic peaks of Mg, O, and C can be found, which points out the high purity of the three MgO samples. Meanwhile, the O 1s high-resolution scans of samples are shown in Figure 7b,d,f. On the low binding energy (BE) side, three samples have two O 1s characteristic peaks at 529 and 531 eV. The characteristic peak at 529 eV is considered to be the lattice oxygen in Mg–O, and the characteristic peak at 531 eV is attributed to the lattice oxygen in Mg–OH [45,46]. This confirms the existence of hydroxyl groups on the surface of MgO, which contributes a little to the catalysis of PMS.

On the high BE side, MgO at 50 nm and MgO at 1 μm have two characteristic peaks near 534 and 532 eV, while only one characteristic peak near 534 eV is found in MgO at 10 μm . The peak located around 534 eV is due to the presence of surface-adsorbed O₂, H₂O, and CO₂, whereas the peak near 532 eV is ascribed to defective sites with low oxygen coordination [47]. Previous studies have shown that the more oxygen vacancies there are on the surface of MgO, the higher the activity [48]. Interestingly, the intensity of characteristic peak at 532 eV is the largest in MgO at 50 nm and the second largest in MgO at 1 μm , meaning the highest and second oxygen vacancy concentration, respectively. However, this peak is absent in MgO at 10 μm , which is because the oxygen vacancy concentration is too low to be detected. In the three kinds of MgO, the oxygen vacancy concentration has an incredible coincidence with the catalytic performances (shown in Figure 2f and Figure S8). Therefore, it can be reasonably concluded that the oxygen vacancy in MgO surface has an important influence on the catalysis of PMS.

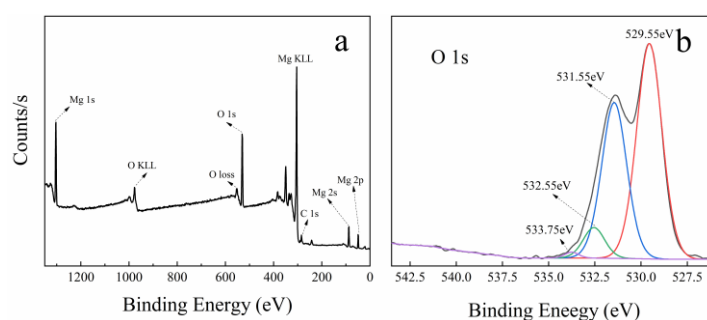


Figure 7. Cont.

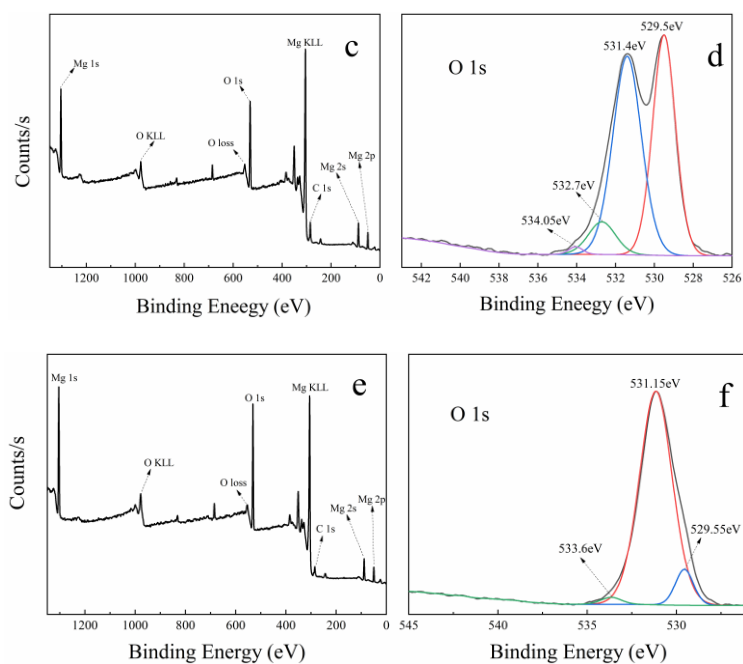


Figure 7. XPS spectra of three kinds of MgO with different particle sizes: (a,b) is 50 nm, (c,d) is 1 μm , and (e,f) is 10 μm . (a,c,e) Full survey spectra; (b,d,f) high-resolution scans of O 1s, respectively.

Optical investigations can reveal very useful information to understand the physical properties of materials [23,49]; as a result, photoluminescence spectroscopy (PL) of three kinds of MgO with different particle sizes are given in Figure 8. With an excitation wavelength of 325 nm, the PL spectra exhibit an intrinsic emission peak at 372 nm, a purple emission resulted from adsorbed oxygen species centered around 400 nm, and two blue emission around 454 and 469 nm, which are attributed to the oxygen vacancy (F center) [50,51]. When the valence band of MgO is excited by light, some of photogenerated electrons are trapped by oxygen vacancies. The electrons eventually fall back to the valence band, producing a new fluorescent peak that is distinct from the intrinsic fluorescence emission peak of MgO. At the same time, the defect level of the oxygen vacancy is lower than the conduction band level, so the new fluorescent emission peak is generally in the right visible region of its intrinsic fluorescence emission peak (e.g., red-shift). Importantly, the more the defect concentration, the higher the luminescence intensity [52]. It is clearly shown that the emission intensity of oxygen vacancy of the MgO at 50 nm is the maximum irrespective of the emission wavelengths, indicating the highest defect concentration in the MgO at 50 nm. The second is the MgO at 1 μm , and the smallest intensity is the MgO at 10 μm . This result is surprisingly like previous catalytic experiments (Figure S8) and XPS results (Figure 7), so it is further determined that oxygen vacancy in the MgO surface is the key factor for MgO-catalyzing PMS.

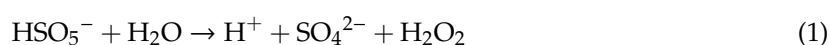


Figure 8. Photoluminescence spectra of three kinds of MgO with different particle sizes.

3.2.4. Probable Catalytic Path

Based on the above experimental and analytical results, we can come to some understandings about the PMS/MgO catalysis system, namely, (1) singlet oxygen is the main active oxygen species produced in PMS/MgO system; (2) singlet oxygen originates from the breaking of peroxide group (–O–O–) in PMS; (3) oxygen vacancy in MgO surface plays a crucially catalytic role to efficiently break peroxide group in PMS. In addition, a small amount of superoxide anion radicals and hydroxyl radicals are also produced in the PMS/MgO system, to degrade organic compounds, and the surface hydroxyl group of MgO also helps catalyze PMS to form active oxygen species.

The hydrogen peroxide produced by hydrolysis of peroxydisulfate molecules generates hydroxyl radical, which immediately reacts with excessive hydrogen peroxide, to generate superoxide anion radical [53]. The hydroxyl radical and superoxide anion radical formed in the previous stage can react and generate singlet oxygen and hydroxyl [54]. Thus, the relevant radical reactions of PMS catalyzed by hydroxyl on MgO can be proposed in Equations (1)–(4):



With the development of nonradical catalysis technology, researchers have found that singlet oxygen is produced in activated PMS by ketones, quinones, carbon materials, and so on. The unsaturated carbon atoms in the carbon material and the carbonyl group in the ketones and quinones are catalytic active sites, acting as intermediate mediators to accelerate the decomposition and interaction of persulfate molecules, to produce singlet oxygen [34]. New findings in this article determine that oxygen vacancies in the surface of MgO are also highly active sites to catalyze PMS. Dong et al. found that the abundant oxygen vacancies not only increased the reducibility of the catalyst, but also facilitated the electron transfer from PMS and organic molecules to the catalyst [55]. Therefore, in the proposed mechanism, based on the abovementioned results and previous reports, we refer to the literature and speculate that oxygen vacancy in the MgO surface acts as mediator, which temporarily receives oxygen atoms of hydroxyl groups on HSO_5^- , and then promotes the breakage of peroxide bands and accelerates the combination of broken oxygen atoms, to form singlet oxygen [56], as shown in Figure 9. It is speculated that the possible path of catalysis of PMS by oxygen vacancy on the MgO surface is presented in Equations (5) to (6).

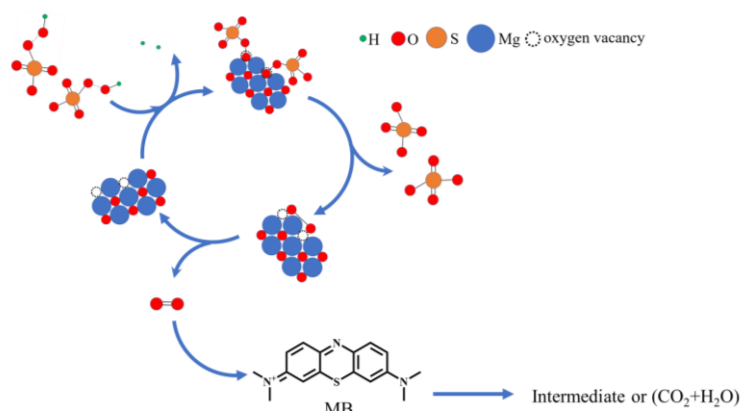
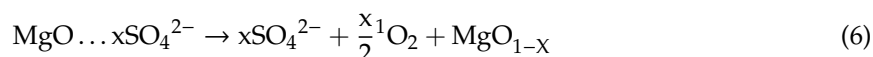
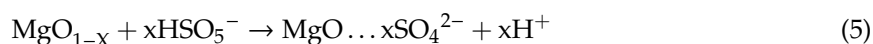


Figure 9. The possible path of PMS catalysis by oxygen vacancy in the surface of MgO.



4. Conclusions

MgO is a highly efficient catalyst for PMS; unfortunately, it was completely neglected. MgO has excellent efficiency and recyclability to catalyze PMS to degrade many organic substances, in a wide pH range. In addition, free radical scavengers and electron-spin-resonance studies have confirmed that singlet oxygen is the key active oxygen species in the PMS/MgO system. More importantly, it has been proved that, in the PMS/MgO system, the oxygen vacancy in the MgO surface plays a crucial role in the catalytic process, which efficiently breaks the peroxide group (–O–O–) in PMS, to produce abundant singlet oxygen in a short time. The good degradation effect, wide pH adaptability, good recovery, easy preparation, and feasible treatment of actual wastewater indicate the good application prospect of MgO. This study shows that MgO is a very promising catalyst for PMS, which can be used to efficiently catalyze the degradation of actual organic wastewater, and promotes the development of persulfate catalyst to some extent.

Supplementary Materials: The following are available online at <http://www.mdpi.com/2075-163X/10/1/2/s1>, Figure S1: X-ray diffraction patterns of three kinds of MgO, Figure S2: X-ray diffraction patterns of MgO before and after reaction, Figure S3: Catalytic degradation of various organic dyes in PMS/MgO system, Figure S4: Effects of the radical scavengers on MB degradation. (a) tert- butanol, (b) methanol (TBA), (c) SOD and (d) furfuryl alcohol. Control conditions: (MB) = 100 mg/L, (PMS) = 0.8 g/L, (MgO) = 0.4 g/L, pH = 7, T = 25 °C, Figure S5: Effect of dissolved oxygen on the degradation of MB by PMS/MgO system. Control condition: (MB) = 100 mg/L, (PMS) = 0.8 g/L, (MgO) = 0.4 g/L, T = 25 °C, pH = 7, Figure S6: The effect of pH on Mg²⁺ concentration in solution, Figure S7: Differences in catalytic effects of MgO with or without calcination in argon. Control conditions: (MB) = 100 mg/L, (PMS) = 0.08 g, (MgO) = 0.04 g, T = 25 °C, pH = 7, Figure S8: The effect of the calcined MgO with different sizes on MB degradation.

Author Contributions: Q.P. performed experiments, analyzed data, and wrote the paper; X.T. analyzed data and co-wrote the paper; K.L. designed experiments, supervised research, and revised the paper; X.L. and D.H. provided positive guidance and help. Y.D. and G.H. performed some catalytic degradation experiments. All authors have read and agreed to the published version of the manuscript.

Funding: This research was funded by the National Natural Science Foundation of China (No. 51774330) and the Fundamental Research Funds for the Central Universities of Central South University (No. 2018zzts 804).

Conflicts of Interest: The authors declare no conflict of interest.

References

- Hameed, B.H.; Din, A.T.M.; Ahmad, A.L. Adsorption of methylene blue onto bamboo-based activated carbon: Kinetics and equilibrium studies. *J. Hazard. Mater.* **2007**, *141*, 819–825. [[CrossRef](#)] [[PubMed](#)]
- Gupta, V.K.; Pathania, D.; Agarwal, S.; Singh, P. Adsorptional photocatalytic degradation of methylene blue onto pectin-CuS nanocomposite under solar light. *J. Hazard. Mater.* **2012**, *243*, 179–186. [[CrossRef](#)] [[PubMed](#)]
- Foo, K.Y.; Hameed, B.H. Preparation, characterization and evaluation of adsorptive properties of orange peel based activated carbon via microwave induced K₂CO₃ activation. *Bioresour. Technol.* **2012**, *104*, 679–686. [[CrossRef](#)] [[PubMed](#)]
- De Gisi, S.; Lofrano, G.; Grassi, M.; Notarnicola, M. Characteristics and adsorption capacities of low-cost sorbents for wastewater treatment: A review. *Sustain. Mater. Technol.* **2016**, *9*, 10–40. [[CrossRef](#)]
- Crini, G. Non-conventional low-cost adsorbents for dye removal: A review. *Bioresour. Technol.* **2006**, *97*, 1061–1085. [[CrossRef](#)]
- Raju, M.D.; Joseph, P.; Kavitha, E.; Dhanasekaran, N.; Grahadurai, H.M.; Mohan, T. Remediation of textile effluents by membrane based treatment techniques: A state of the art review. *J. Chem. Pharm. Sci.* **2014**, *147*, 296–299.

7. Liang, C.Z.; Sun, S.P.; Li, F.Y.; Ong, Y.K.; Chung, T.S. Treatment of highly concentrated wastewater containing multiple synthetic dyes by a combined process of coagulation/flocculation and nanofiltration. *J. Memb. Sci.* **2014**, *469*, 306–315. [[CrossRef](#)]
8. Li, Z.; Tang, X.; Liu, K.; Huang, J.; Xu, Y.; Peng, Q.; Ao, M. Synthesis of a $\text{MnO}_2/\text{Fe}_3\text{O}_4$ /diatomite nanocomposite as an efficient heterogeneous Fenton-like catalyst for methylene blue degradation. *Beilstein J. Nanotechnol.* **2018**, *9*, 1940–1950. [[CrossRef](#)]
9. Qi, C.; Liu, X.; Ma, J.; Lin, C.; Li, X.; Zhang, H. Activation of peroxymonosulfate by base: Implications for the degradation of organic pollutants. *Chemosphere* **2016**, *151*, 280–288. [[CrossRef](#)]
10. Indrawirawan, S.; Sun, H.; Duan, X.; Wang, S. Nanocarbons in different structural dimensions (0–3D) for phenol adsorption and metal-free catalytic oxidation. *Appl. Catal. B Environ.* **2015**, *179*, 352–362. [[CrossRef](#)]
11. Sillanpää, M.; Ncibi, M.C.; Matilainen, A. Advanced oxidation processes for the removal of natural organic matter from drinking water sources: A comprehensive review. *J. Environ. Manag.* **2018**, *208*, 56–76. [[CrossRef](#)]
12. Wang, Y.; Sun, H.; Ang, H.M.; Tadó, M.O.; Wang, S. Facile synthesis of hierarchically structured magnetic $\text{MnO}_2/\text{ZnFe}_2\text{O}_4$ hybrid materials and their performance in heterogeneous activation of peroxymonosulfate. *ACS Appl. Mater. Interfaces* **2014**, *6*, 19914–19923. [[CrossRef](#)]
13. Liu, J.; Zhao, Z.; Shao, P.; Cui, F. Activation of peroxymonosulfate with magnetic Fe_3O_4 - MnO_2 core-shell nanocomposites for 4-chlorophenol degradation. *Chem. Eng. J.* **2015**, *262*, 854–861. [[CrossRef](#)]
14. Anipsitakis, G.P.; Dionysiou, D.D. Radical generation by the interaction of transition metals with common oxidants. *Environ. Sci. Technol.* **2004**, *38*, 3705–3712. [[CrossRef](#)] [[PubMed](#)]
15. Luo, S.; Duan, L.; Sun, B.; Wei, M.; Li, X.; Xu, A. Manganese oxide octahedral molecular sieve (OMS-2) as an effective catalyst for degradation of organic dyes in aqueous solutions in the presence of peroxymonosulfate. *Appl. Catal. B Environ.* **2015**, *164*, 92–99. [[CrossRef](#)]
16. Qi, C.; Liu, X.; Lin, C.; Zhang, X.; Ma, J.; Tan, H.; Ye, W. Degradation of sulfamethoxazole by microwave-activated persulfate: Kinetics, mechanism and acute toxicity. *Chem. Eng. J.* **2014**, *249*, 6–14. [[CrossRef](#)]
17. Zhu, S.; Huang, X.; Ma, F.; Wang, L.; Duan, X.; Wang, S. Catalytic Removal of Aqueous Contaminants on N-Doped Graphitic Biochars: Inherent Roles of Adsorption and Nonradical Mechanisms. *Environ. Sci. Technol.* **2018**, *52*, 8649–8658. [[CrossRef](#)]
18. Fan, J.; Qin, H.; Jiang, S. Mn-doped $\text{g-C}_3\text{N}_4$ composite to activate peroxymonosulfate for acetaminophen degradation: The role of superoxide anion and singlet oxygen. *Chem. Eng. J.* **2019**, *359*, 723–732. [[CrossRef](#)]
19. Tang, X.; Huang, J.; Liu, K.; Feng, Q.; Li, Z.; Ao, M. Synthesis of magnetically separable $\text{MnO}_2/\text{Fe}_3\text{O}_4$ /silica nanofiber composite with enhanced Fenton-like catalytic activity for degradation of Acid Red 73. *Surf. Coat. Technol.* **2018**, *354*, 18–27. [[CrossRef](#)]
20. Tang, X.; Feng, Q.; Liu, K.; Li, Z.; Wang, H. Fabrication of magnetic Fe_3O_4 /silica nanofiber composites with enhanced Fenton-like catalytic performance for Rhodamine B degradation. *J. Mater. Sci.* **2018**, *53*, 369–384. [[CrossRef](#)]
21. Huang, Z.; Chen, Z.; Chen, Y.; Hu, Y. Synergistic effects in iron-copper bimetal doped mesoporous $\gamma\text{-Al}_2\text{O}_3$ for Fenton-like oxidation of 4-chlorophenol: Structure, composition, electrochemical behaviors and catalytic performance. *Chemosphere* **2018**, *203*, 442–449. [[CrossRef](#)] [[PubMed](#)]
22. Li, C.; Huang, Y.; Dong, X.; Sun, Z.; Duan, X.; Ren, B.; Zheng, S.; Dionysiou, D.D. Highly efficient activation of peroxymonosulfate by natural negatively-charged kaolinite with abundant hydroxyl groups for the degradation of atrazine. *Appl. Catal. B Environ.* **2019**, *247*, 10–23. [[CrossRef](#)]
23. Anpo, M.; Yamada, Y.; Kubokawa, Y.; Coluccia, S.; Zecchina, A.; Che, M. Photoluminescence properties of MgO powders with coordinatively unsaturated surface ions. *J. Chem. Soc. Faraday Trans. 1 Phys. Chem. Condens. Phases* **1988**, *84*, 751–764. [[CrossRef](#)]
24. Li, Z.; Tang, X.; Liu, K.; Huang, J.; Peng, Q.; Ao, M.; Huang, Z. Fabrication of novel sandwich nanocomposite as an efficient and regenerable adsorbent for methylene blue and Pb (II) ion removal. *J. Environ. Manag.* **2018**, *218*, 363–373. [[CrossRef](#)] [[PubMed](#)]
25. Khan, J.A.; He, X.; Khan, H.M.; Shah, N.S.; Dionysiou, D.D. Oxidative degradation of atrazine in aqueous solution by $\text{UV}/\text{H}_2\text{O}_2/\text{Fe}^{2+}$, $\text{UV}/\text{S}_2\text{O}_8^{2-}/\text{Fe}^{2+}$ and $\text{UV}/\text{HSO}_5^-/\text{Fe}^{2+}$ processes: A comparative study. *Chem. Eng. J.* **2013**, *218*, 376–383. [[CrossRef](#)]
26. Lange, A.; Brauer, H.-D. On the formation of dioxiranes and of singlet oxygen by the ketone-catalysed decomposition of Caro's acid. *J. Chem. Soc.* **1996**, *5*, 208. [[CrossRef](#)]

27. Vyazovkin, S. On the phenomenon of variable activation energy for condensed phase reactions. *New J. Chem.* **2000**, *24*, 913–917. [[CrossRef](#)]
28. Guan, Y.-H.; Ma, J.; Li, X.-C.; Fang, J.-Y.; Chen, L.-W. Influence of pH on the Formation of Sulfate and Hydroxyl Radicals in the UV/Peroxymonosulfate System. *Environ. Sci. Technol.* **2011**, *45*, 9308–9314. [[CrossRef](#)]
29. Bindhu, M.R.; Umadevi, M.; Kavin Micheal, M.; Arasu, M.V.; Abdullah Al-Dhabi, N. Structural, morphological and optical properties of MgO nanoparticles for antibacterial applications. *Mater. Lett.* **2016**, *166*, 19–22. [[CrossRef](#)]
30. Monteagudo, J.M.; El-taliawy, H.; Durán, A.; Caro, G.; Bester, K. Sono-activated persulfate oxidation of diclofenac: Degradation, kinetics, pathway and contribution of the different radicals involved. *J. Hazard. Mater.* **2018**, *357*, 457–465. [[CrossRef](#)]
31. Zhang, D.; Wu, L.; Yao, J.; Herrmann, H.; Richnow, H.H. Carbon and hydrogen isotope fractionation of phthalate esters during degradation by sulfate and hydroxyl radicals. *Chem. Eng. J.* **2018**, *347*, 111–118. [[CrossRef](#)]
32. Sannasimuthu, A.; Kumaresan, V.; Pasupuleti, M.; Paray, B.A.; Al-Sadoon, M.K.; Arockiaraj, J. Radical scavenging property of a novel peptide derived from C-terminal SOD domain of superoxide dismutase enzyme in *Arthrospira platensis*. *Algal Res.* **2018**, *35*, 519–529. [[CrossRef](#)]
33. Appiani, E.; Ossola, R.; Latch, D.E.; Erickson, P.R.; Mcneill, K. Aqueous singlet oxygen reaction kinetics of furfuryl alcohol: Effect of temperature, pH, and salt content. *Environ. Sci. Process Impacts* **2017**, *19*, 507–516. [[CrossRef](#)] [[PubMed](#)]
34. Zhou, Y.; Jiang, J.; Gao, Y.; Ma, J.; Pang, S.Y.; Li, J.; Lu, X.T.; Yuan, L.P. Activation of Peroxymonosulfate by Benzoquinone: A Novel Nonradical Oxidation Process. *Environ. Sci. Technol.* **2015**, *49*, 12941–12950. [[CrossRef](#)]
35. Bu, L.; Ding, J.; Zhu, N.; Kong, M.; Wu, Y.; Shi, Z.; Zhou, S.; Dionysiou, D.D. Unraveling different mechanisms of persulfate activation by graphite felt anode and cathode to destruct contaminants of emerging concern. *Appl. Catal. B Environ.* **2019**, *253*, 140–148. [[CrossRef](#)]
36. Li, H.; Shan, C.; Li, W.; Pan, B. Peroxymonosulfate activation by iron(III)-tetraamidomacrocyclic ligand for degradation of organic pollutants via high-valent iron-oxo complex. *Water Res.* **2018**, *147*, 233–241. [[CrossRef](#)] [[PubMed](#)]
37. Fontmorin, J.M.; Burgos Castillo, R.C.; Tang, W.Z.; Sillanpää, M. Stability of 5, 5-dimethyl-1-pyrroline-N-oxide as a spin-trap for quantification of hydroxyl radicals in processes based on Fenton reaction. *Water Res.* **2016**, *99*, 24–32. [[CrossRef](#)]
38. Mendoza, C. Heterogeneous singlet oxygen generation: In-operando visible light EPR spectroscopy. *Environ. Sci. Pollut. Res.* **2019**, *2019*, 1–6. [[CrossRef](#)]
39. Wu, Q.; He, Z.; Wang, X.; Zhang, Q.; Wei, Q.; Ma, S.; Ma, C.; Li, J.; Wang, Q. Cascade enzymes within self-assembled hybrid nanogel mimicked neutrophil lysosomes for singlet oxygen elevated cancer therapy. *Nat. Commun.* **2019**, *10*, 1–14. [[CrossRef](#)]
40. Li, X.; Liu, J.; Rykov, A.I.; Han, H.; Jin, C.; Liu, X.; Wang, J. Excellent photo-Fenton catalysts of Fe-Co Prussian blue analogues and their reaction mechanism study. *Appl. Catal. B Environ.* **2015**, *179*, 196–205. [[CrossRef](#)]
41. Chen, C.-Y.; Jafvert, C.T. Photoreactivity of Carboxylated Single-Walled Carbon Nanotubes in Sunlight: Reactive Oxygen Species Production in Water. *Environ. Sci. Technol.* **2010**, *44*, 6674–6679. [[CrossRef](#)] [[PubMed](#)]
42. Hollerer, M.; Prochinig, D.; Puschnig, P.; Carrasco, E.; Freund, H.-J.; Sterrer, M. Scanning Tunneling Microscopy of the Ordered Water Monolayer on MgO (001)/Ag (001) Ultrathin Films. *J. Phys. Chem. C* **2019**, *123*, 3711–3718. [[CrossRef](#)]
43. Raghupathi, K.R.; Koodali, R.T.; Manna, A.C. Size-Dependent Bacterial Growth Inhibition and Mechanism of Antibacterial Activity of Zinc Oxide Nanoparticles. *Langmuir* **2011**, *27*, 4020–4028. [[CrossRef](#)] [[PubMed](#)]
44. Aswal, D.K.; Muthe, K.P.; Tawde, S.; Chodhury, S.; Bagkar, N.; Singh, A.; Gupta, S.K.; Yakhmi, J. V XPS and AFM investigations of annealing induced surface modifications of MgO single crystals. *J. Cryst. Growth* **2002**, *236*, 661–666. [[CrossRef](#)]
45. Zhang, Y.; Zhao, Z.; Chen, J.; Cheng, L.; Chang, J.; Sheng, W.; Hu, C.; Cao, S. C-doped hollow TiO₂ spheres: In situ synthesis, controlled shell thickness, and superior visible-light photocatalytic activity. *Appl. Catal. B Environ.* **2015**, *165*, 715–722. [[CrossRef](#)]

46. Dong, F.; Guo, S.; Wang, H.; Li, X.; Wu, Z. Enhancement of the Visible Light Photocatalytic Activity of C-Doped TiO₂ Nanomaterials Prepared by a Green Synthetic Approach. *J. Phys. Chem. C* **2011**, *115*, 13285–13292. [[CrossRef](#)]
47. Fang, G.; Zhou, J.; Cai, Y.; Liu, S.; Tan, X.; Pan, A.; Liang, S. Metal-organic framework-templated two-dimensional hybrid bimetallic metal oxides with enhanced lithium/sodium storage capability. *J. Mater. Chem. A* **2017**, *5*, 13983–13993. [[CrossRef](#)]
48. Aničić, N.; Vukomanović, M.; Koklič, T.; Suvorov, D. Fewer Defects in the Surface Slows the Hydrolysis Rate, Decreases the ROS Generation Potential, and Improves the Non-ROS Antimicrobial Activity of MgO. *Small* **2018**, *14*, 1–12.
49. Ao, M.; Liu, K.; Tang, X.; Li, Z.; Peng, Q.; Huang, J. BiOCl/TiO₂/diatomite composites with enhanced visible-light photocatalytic activity for the degradation of rhodamine B. *Beilstein J. Nanotechnol.* **2019**, *10*, 1412–1422. [[CrossRef](#)]
50. Zhang, J.; Zhang, L. Intensive green light emission from MgO nanobelts. *Chem. Phys. Lett.* **2002**, *363*, 293–297. [[CrossRef](#)]
51. Hao, Y.J.; Liu, B.; Tian, L.G.; Li, F.T.; Ren, J.; Liu, S.J.; Liu, Y.; Zhao, J.; Wang, X.J. Synthesis of {111} Facet-Exposed MgO with Surface Oxygen Vacancies for Reactive Oxygen Species Generation in the Dark. *ACS Appl. Mater. Interfaces* **2017**, *9*, 12687–12693. [[CrossRef](#)] [[PubMed](#)]
52. Wang, S.; Chen, P.; Bai, Y.; Yun, J.H.; Liu, G.; Wang, L. New BiVO₄ Dual Photoanodes with Enriched Oxygen Vacancies for Efficient Solar-Driven Water Splitting. *Adv. Mater.* **2018**, *30*, 1–7. [[CrossRef](#)] [[PubMed](#)]
53. Burns, J.M.; Cooper, W.J.; Ferry, J.L.; King, D.W.; DiMento, B.P.; McNeill, K.; Miller, C.J.; Miller, W.L.; Peake, B.M.; Rusak, S.A.; et al. Methods for reactive oxygen species (ROS) detection in aqueous environments. *Aquat. Sci.* **2012**, *74*, 683–734. [[CrossRef](#)]
54. Liu, X.; Zhang, X.; Zhang, K.; Qi, C. Chemosphere Sodium persulfate-assisted mechanochemical degradation of tetrabromobisphenol A: Efficacy, products and pathway. *Chemosphere* **2016**, *150*, 551–558. [[CrossRef](#)] [[PubMed](#)]
55. Dong, X.; Duan, X.; Sun, Z.; Zhang, X.; Li, C. Applied Catalysis B: Environmental Natural illite-based ultrafine cobalt oxide with abundant oxygen-vacancies for highly efficient Fenton-like catalysis. *Appl. Catal. B Environ.* **2020**, *261*, 118214. [[CrossRef](#)]
56. Zhang, T.; Chen, Y.; Wang, Y.; Le Roux, J.; Yang, Y.; Croué, J.P. Efficient peroxydisulfate activation process not relying on sulfate radical generation for water pollutant degradation. *Environ. Sci. Technol.* **2014**, *48*, 5868–5875. [[CrossRef](#)] [[PubMed](#)]



© 2019 by the authors. Licensee MDPI, Basel, Switzerland. This article is an open access article distributed under the terms and conditions of the Creative Commons Attribution (CC BY) license (<http://creativecommons.org/licenses/by/4.0/>).